ELSEVIER

Materials Chemistry and Physics 50 (1997) 200–204

MATERIALS CHEMISTRY AND PHYSICS

Simulation and analysis of the capacitance–voltage characteristics of the δ-doped semiconductors

D.G. Liu [a,*], C.P. Lee [b]

[a] *Department of Electronic Engineering, Feng Chia University, Taichung, Taiwan, ROC*
[b] *Institute of Electronics, Chiao Tung University, Hsinchu, Taiwan, ROC*

Received 19 December 1996; revised 27 February 1997

Abstract

In this paper, a self-consistent model to simulate the general characteristics of one-dimensional semiconductor structures is demonstrated. During calculation, possible quantum effects and the distributions of both electrons and holes are all considered. In this model, a continuity equation is solved to calculate the distribution of free electrons and holes. The possible quantum wells are sought using the Schrödinger equation. The overall charge density and potential are obtained self-consistently by an iteration scheme. The *C–V* characteristics of the δ-doped structures are simulated and then compared with those of practical samples. By comparing with these δ-doped samples, the effective numbers of dopant atoms can be precisely determined. For these highly doped samples, it is found that the activation rates are only about half. This finding can be verified by Hall measurements which confirms the accuracy in this study. © 1997 Elsevier Science S.A.

Keywords: Delta-doping; Quantum wells; Self-consistent calculation; Doping concentration; *C–V* characteristics

1. Introduction

In past years, δ-doped devices have attracted a great deal of attention because of their substantial advantages in device applications and the embedded physics within them. Owing to the capability of epitaxial equipment to grow very thin layers, there is keen interest to confine carriers and impurities in a very narrow region. To form a δ-doped layer, a large number of dopant atoms, usually Si and Be for n- and p-type compound semiconductors respectively, are deposited while the growth of the host materials is interrupted. After depositing a large number of dopant atoms on the surface, the growth mode is reinstated to sandwich the dopants in the epilayer. Such a δ-doping technique can be applied in molecular beam epitaxy (MBE) and other growth techniques such as metal–organic chemical vapor deposition and metal organic MBE [1,2]. Several high speed and optoelectronic devices, e.g. the δ-doped channel field effect transistor [3,4], bipolar transistor [5], ultrafast pulse generator [6], and low-noise photodiode [7], have been designed by incorporating δ-doped structures to improve their performances.

With the development of advanced applications in various electronic devices, good control of the active doping density and a finite spread of the δ-doped layer are of concern in the device structures. This requires a good understanding the properties of the δ-doped layers. Methods of direct measurement are secondary ion mass spectrometry and *C–V* analysis, which reflect the distribution of dopants and charges [8]. The related energy band structure of the V-shapes well formed in the δ-doped layers has also been studied. Several characterization techniques such as photoluminescence and deep level transient spectroscopy accompanied by theoretical studies have been utilized to analyze the δ-doped structures [9–13]. These studies usually consider only the Schrödinger equation coupled with the Poisson equation to achieve a self-consistent result at low temperatures [9–12,14–16]. Agreement between the numerical calculations and measurements has been achieved. However, a more general-purpose simulation tool which can consider both the quantized and the free carriers simultaneously is still unavailable for a wider range of measurements, e.g. the electrical characteristics and measurements under various biases or at a higher temperature.

In this paper, a home-made simulation tool is used to calculate the general characteristics of one-dimensional semiconductor structures. During the calculation, possible quantum wells are sought. The distributions of both electrons and holes are included. In the present study, the finite difference formula is used in the discretization scheme.

* Corresponding author.

0254-0584/97/$17.00 © 1997 Elsevier Science S.A. All rights reserved
PII S0254-0584(97)01919-6

Using this tool, the simulated *C–V* characteristics of δ-doped semiconductors are compared with measured data. Since the δ-doped structures are formed by inserting a sheet of dopants in the host material, the impurity atoms are largely confined within a few monolayers. A flat region will be found in the *C–V* curves during depletion through this δ-doped layer. By tuning the device area and its effective impurity concentration in our calculation, *C–V* curves and charge distributions that are very close to those of the real devices can be obtained. It is found that, under the condition of high doping concentration, the fitted doses are much lower than those intentionally doped in the samples. This finding is attributed to the limited solubility of Si in GaAs. In contrast, the solubility of Si in InGaAs is higher than that in GaAs with the same nominal doping concentration. With a double check from Hall measurements, the fitted results are believed to be very accurate.

2. Self-consistent model

In this model, a continuity equation is solved to calculate the distribution of free carriers. Possible quantum wells in the devices are sought. The distribution of these quantized carriers is obtained from the Schrödinger equation. Therefore, the total charge density considered in the whole structure includes free, quantized carriers and ionized impurities. However, the overall charge distribution and the potential profile are affected by each other. The resulting charge distribution and potential profile must satisfy the Poisson equation, the continuity equation and Schrödinger equation simultaneously.

Fig. 1 shows the flow chart of our calculation. Three equations, the Schrödinger equation, the continuity equation and the Poisson equation, are coupled to achieve a convergent result on iteration. An iterative scheme similar to that proposed in Ref. [17] is used to accelerate the speed of convergence. A trial potential, Φ_{in}, is first assumed; this is simply calculated from the continuity equation and the Poisson equation. For a given potential, the quantum wells are sought to see if there are possible quantized states with energies below the barriers. The energy spectrum above the barriers is presumed to be continuous. And those carriers occupying these unbounded states are taken as free carriers. These quantized carriers, i.e. n_{2D} and p_{2D} in Fig. 1, and free carriers, n_{3D} and p_{3D}, are obtained from the Schrödinger equation and the continuity equation respectively. Before summing up all charged particles, carrier concentrations are normalized to ensure neutrality of the total charges is satisfied. This process is helpful for stably converging calculations, especially under conditions of high doping concentrations. In the case of high doses, a small variation of potential will cause large variations in the carrier concentrations owing to the exponential characteristics of the Fermi probability. Such changes of charge densities will feed back to cause a large changed potential, and therefore oscillatory or divergent calculations will occur. Such renormalization will ensure a more stable adjustment in potential and charges to prevent the above unsatisfactory conditions. To solve these one-dimensional differential equations, the finite difference method is used in the discretization scheme. After solving the three governing equations, another potential Φ_{out} will be obtained. If Φ_{in} is equal to Φ_{out}, the calculated potential and charge profiles are the self-consistent solutions of the three governing equations. In usual cases, the potential is not easily tried out. An iterative scheme is then applied to find the converged solutions. A new trial potential is a linear combination of the original potential Φ_{in} and the resulting potential from the Poisson equation, i.e.

$$\Phi'_{in} = (1-f)\,\Phi_{in} + f\Phi_{out} \tag{1}$$

The convergence factor f is changed dynamically over a range of less than 0.8 for quick convergence.

After the calculations have converged, the specific characteristics such as current or capacitance under a bias are derived. Fig. 2 shows typical calculation results for a δ-doped InGaAs well under a forward bias. This program provides complete information inside the semiconductors. In this case, quasi-Fermi levels of both electrons and holes are obtained and are found to be split. Since the n-type dopants are deposited in the center of the quantum well, most electrons are confined in the well. The density of holes is too low to be seen in this figure.

To obtain the capacitance of a δ-doped sample under a specific bias, the relation between the surface sheet charge n_s and the biases is first evaluated, i.e.

$$n_s(V) = \frac{\varepsilon_s}{q} F_s(V) \tag{2}$$

The equivalent capacitance can be obtained by differentiating the above relation, i.e.

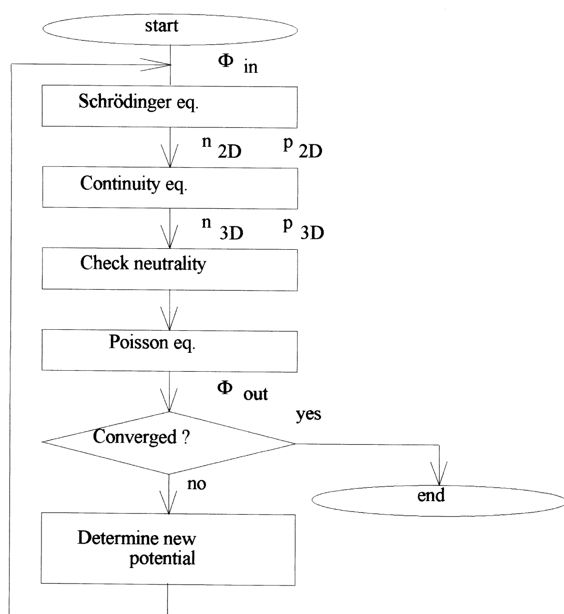

Fig. 1. Flow chart of the self-consistent calculation.

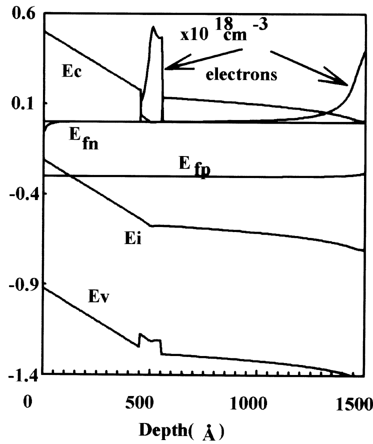

Fig. 2. The simulated potential profiles, quasi-Fermi energies, and electron distributions of a δ-doped InGaAs well at a bias of 0.3 V.

$$C(V)=\frac{\mathrm{d}}{\mathrm{d}V}n_s(V) \tag{3}$$

These *C–V* characteristics are then compared with those of practical samples.

3. Sample preparation

In this paper, two device structures are studied as shown in Fig. 3. The first structure is conventional δ-doped GaAs with two doping concentrations, i.e. 8.3×10^{11} cm^{-2} and 3.3×10^{12} cm^{-2}. The other structure is a δ-doped InGaAs sandwiched by GaAs. The actual concentration of impurities in the doped layers was extracted with the help of simulation.

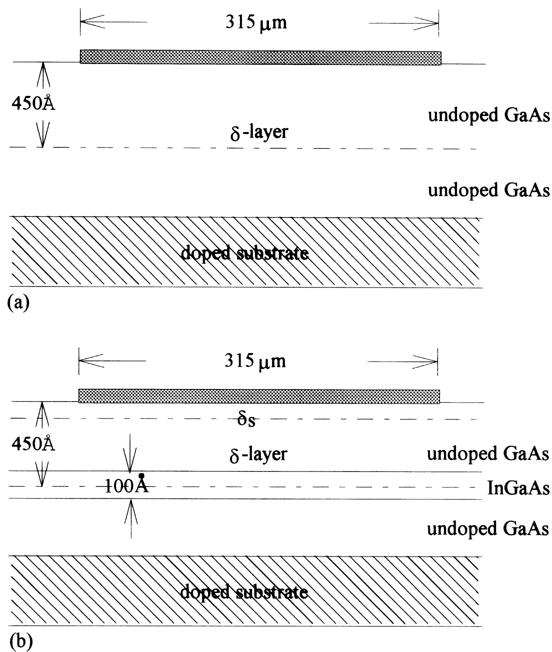

Fig. 3. Schematic diagrams of the δ-doped structures used in calculation: (a) δ-doped GaAs; (b) δ-doped GaAs/$In_{0.15}Ga_{0.85}As$/GaAs quantum well. The substrate is doped by a concentration of 2×10^{18} cm^{-3} for the ohmic contact. The surface Schottky contact is defined by an Al plate.

The effect of heterojunctions was investigated. All the samples were grown by solid source MBE under normal growth conditions. Only the growth temperatures were different: 580°C and 480°C for GaAs and InGaAs respectively.

The capacitance curves of each sample were measured at room temperature with an HP4192 apparatus at a frequency of 50 kHz. The apparent charge profiles are also derived from the *C–V* curves by the conventional techniques, i.e.

$$d=\varepsilon_s/C \tag{4}$$

$$N(d)=\frac{C^3}{q\varepsilon_s}\frac{\mathrm{d}V}{\mathrm{d}C} \tag{5}$$

where C is the measured capacitance under the bias V, $N(d)$ is the apparent density at the depth d, and ε_s is the permittivity of the depleted layer.

4. Results and discussion

During comparison of the *C–V* curves obtained from the calculation and measurement, the effective contact area can be determined, which reveals the lateral depletion at the fringes. Fig. 4 shows typical *C–V* curves of a sample. The effective doping concentration can be roughly selected in this step. However, a more precise determination of the effective concentration in the doped layer is performed by comparing the charge profiles derived from the *C–V* curves. As shown in Fig. 5 for the δ-doped GaAs, with several trial doses by simulation, very close agreement of charge distributions can be obtained. The extracted results are summarized in Table 1.

In Table 1, the intended doping concentrations are listed for comparison. In the case of the low concentration of 8.3×10^{11} cm^{-2}, it is found all the dopants are activated. However, this is not the case in the samples with a higher doping concentration of 3.3×10^{12} cm^{-2}. As seen in Table 1, the fitted doses are much less than those nominally doped. The primary reason may be the limited solubility of the impurity in semiconductors. The amphoteric properties of Si in the compound semiconductors will make the condition worse. A portion of Si atoms act as p-type dopants in the cases of heavy

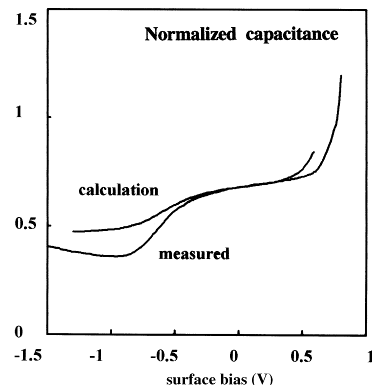

Fig. 4. Normalized *C–V* curves of a δ-doped GaAs. The unit of vertical axis is F m^{-2}.

Table 1
The estimated parameters for each sample

Sample	δ-doped GaAs	δ-doped GaAs	δ-doped InGaAs well
Intended dose	8.3×10^{11} cm^{-2}	3.3×10^{12} cm^{-2}	3.3×10^{12} cm^{-2}
Fitted dose	8.3×10^{11} cm^{-2}	1.75×10^{12} cm^{-2}	2.5×10^{12} cm^{-2}
Total charge (Hall)	–	0.9×10^{12} cm^{-2}	1.5×10^{12} cm^{-2}

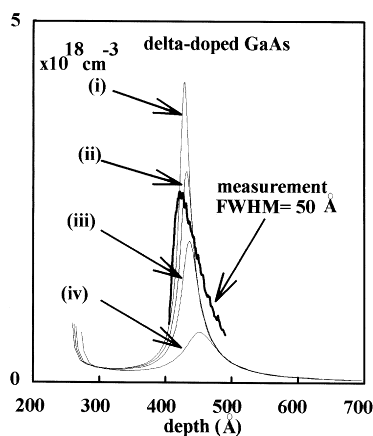

Fig. 5. Derived charge profiles of a δ-doped GaAs from the measurement and the calculations with several trial doses. Curves (i)–(iv) are calculations with doses of 2.0×10^{12} cm^{-2}, 1.75×10^{12} cm^{-2}, 1.5×10^{12} cm^{-2} and 1.0×10^{12} cm^{-2}, respectively. The best-fitted dose is 1.75×10^{12} cm^{-2}.

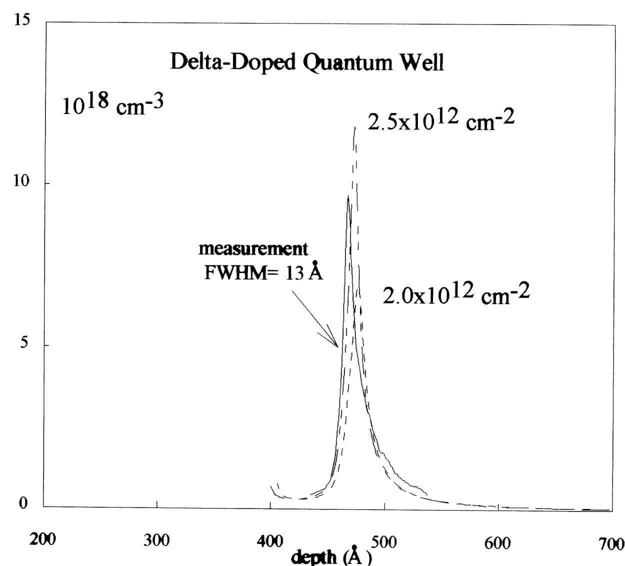

Fig. 6. Charge distributions of the δ-doped InGaAs quantum well from the measurement and the calculations. The effective doping concentration is about 2.5×10^{12} cm^{-2}.

doping. In this case, the effective doping concentration will be compensated. Even with the same nominal dose, it is also found that the δ-doped InGaAs quantum well will have a higher effective dopant density than that for δ-doped GaAs. This fact indicates that the solubility of Si may be higher in InGaAs. Another reason may be the lower growth temperature of InGaAs which reduces the desorption rate of Si during deposition.

Considering the charge profile of the δ-doped InGaAs quantum well, as shown in Fig. 6, it is found the profile is very narrow compared with that for δ-doped GaAs without heterojunctions. The very narrow distribution of the apparent charge profile can be attributed to the confinement enhanced by the heterojunctions.

In Figs. 5 and 6, comparing the apparent charge distributions derived from the simulated *C–V* curves, there is an interesting phenomenon that the peak positions of each profile vary as the doping concentration changes even though the doping location and contact area for each calculation are the same. This finding indicates that the conventional *C–V* profiling technique, Eqs. (4) and (5), cannot truly reflect the doping profiles of the δ-doped structures. Taking δ-doped InGaAs as an example, the above conclusion is manifested by comparing the direct calculated charge profile as shown in Fig. 2 and the derived charge profiles in Fig. 6. These two charge distributions are not the same. Considering Eq. (5), since the derived density $N(d)$ is a function of the slope of the *C–V* curves, $N(d)$ may also indicate the variation of the effective depletion depth d while depleting the δ-doped layer. The higher $N(d)$ we find, the more slowly moving is the depletion depth. Since the δ-doped layer is depleted by separating the conduction band and Fermi level, in the process of depletion the layer will not partially depleted to maintain a definite depleted–undepleted interface. Therefore, the apparent profile $N(d)$ is less related to the physical peak position of carrier concentration.

Considering Fig. 5, it is also found that the tails on the right-hand side of each profile $N(d)$ are almost the same. This means that the curvatures of the calculated *C–V* curves are similar after the δ-layer has been depleted no matter what the doping concentration is. This explanation will indicate that, after the δ-doped layer has been almost depleted, the movements of the effective depletion depth down into the substrate are the same and will not be affected by the depleted layers. This explanation is consistent with the physical meanings. The same tailing of $N(d)$ indicates that the δ-layers are depleted at the same position. It is the same in the case of the δ-doped InGaAs well as shown in Fig. 6. Investigation of the tailing of a real device in Fig. 5 may indicate that the real doping profile is a kind of broadening into the substrate. This finding may be attributed to the thermal diffusion of the impurities during the long period of deposition. In conclusion, the charge profiles of the δ-doped structures derived by the *C–V* characteristics cannot reflect the real charge distribution but rather the degree of confinement of carriers.

The accuracy of the fitted doses can be further confirmed by comparing the results of Hall measurements. As seen in Table 1, the fitted doses are higher than the resulted Hall measurement data. However, these data show the same trend. The lower concentrations obtained by Hall measurements can be attributed to the depletion by Fermi level pinning at the GaAs surface. It is believed that the extracted dose concentrations are very accurate.

5. Conclusion

In this paper, a one-dimensional simulation tool was developed to study general properties of semiconductors, especially those structures with quantum wells. The *C–V* characteristics of several δ-doped samples were investigated. Very close results can be simulated with accurate impurity concentrations. While the impurity dose is as high as 3×10^{13} cm^{-2}, it is found that the actual doping density will be reduced. The effective density depends on the intended doping concentration and materials. In our study, heterojunctions can be used to improve the confinement of carriers.AcknowledgementsThe authors wish to thank the National Science Council of the Republic of China for financial support. The National Center for High–Performance Computing (NCHC) is also acknowledged for providing the computing resources.

Acknowledgements

The authors wish to thank the National Science Council of the Republic of China for financial support. The National Center for High-Performance Computing (NCHC) is also acknowledged for providing the computing resources.

References

[1] C.E.C. Wood, G.M. Metze, J.D. Berry and L.F. Eastman, *J. Appl. Phys., 51* (1) (1980) 383.
[2] T. Kikkawa, T. Ohori, H. Tanaka, K. Kasai and J. Komeno, *J. Cryst. Growth, 115* (448) 1991.
[3] E.F. Schubert, J.E. Cunningham, W.T. Tsang and G.L. Timp, *Appl. Phys. Lett., 51* (15) (1987) 1170.
[4] A.P. Young, J. Chen and H.H. Wieder, *Appl. Phys. Lett., 65* (12) (1994) 1546.
[5] K.W. Goossen, T.Y. Kuo, J.E. Cunningham, W.Y. Jan, F. Ren and C.G. Fanstad, *IEEE Trans. Electron. Dev., 38* (11) (1991) 2423.
[6] D.W. van der Weide, *Appl. Phys. Lett., 65* (7) (1994) 881.
[7] Y. Wang and K.F. Brennan, *IEEE J. Quantum Electron., 30* (5) (1994) 1156.
[8] H.C. Nutt, R.S. Smith, M. Towers, P.K. Rees and D.J. James, *J. Appl. Phys., 70* (2) (1991) 821.
[9] T.W. Kim, Y. Kim and S.-K. Min, *Thin Solid Films, 254* (1995) 61.
[10] A.J. Dewdney, S. Holmes, H. Yu, M. Fahy and R. Murray, *Superlatt. Microstruct., 14* (2–3), (1993) 205.
[11] Q.S. Zhu, Z.T. Zhong, L.W. Lu and C.F. Li, *Appl. Phys. Lett., 65* (19) (1994) 2425.
[12] D.G. Liu, K.H. Chang, C.P. Lee, T.M. Shu and Y.C. Tien, *J. Appl. Phys., 72* (4) (1992) 1468.
[13] D. Birkedal, O. Hansen, C.B. Sørensen, K. Jarasiunas, S.D. Brorson and S.R. Keiding, *Appl. Phys. Lett., 65* (1) (1994) 79.
[14] F. Dominguez-Adame, B. Méndez and E, Maciá, *Semicond. Sci. Technol., 9* (1994) 263.
[15] B. Jogai, P.W. Yu and D.C. Streit, *J. Appl. Phys., 75* (3) (1994) 1586.
[16] M. Ke, D. Westwood, R.H. Williams and M.J. Godfrey, *Phys. Rev. B, 51* (8) (1995) 5038.
[17] F. Stern, *J. Comput. Phys., 6* (1970) 56.